ACS Energy LETTERS

http://pubs.acs.org/journal/aelccp

Revealing the Dual-Layered Solid Electrolyte Interphase on Lithium Metal Anodes via Cryogenic Electron Microscopy

Tae-Ung Wi, Sung O Park, Su Jeong Yeom, Min-Ho Kim, Imanuel Kristanto, Haotian Wang, Sang Kyu Kwak,* and Hyun-Wook Lee*

Cite This: *ACS Energy Lett.* 2023, 8, 2193−2200

Read Online

ACCESS | Metrics & More | Article Recommendations | Supporting Information

ABSTRACT: **It is crucial to comprehend the effect of the solid electrolyte interphase (SEI) on battery performance to develop stable Li metal batteries. Nonetheless, the exact nanostructure and working mechanisms of the SEI remain obscure. Here, we have investigated the relationship between electrolyte components and the structural configuration of interfacial layers using an optimized cryogenic transmission electron microscopy (Cryo-TEM) analysis and theoretical calculation. We revealed a unique dual-layered inorganic-rich nanostructure, in contrast to the widely known simple specific component-rich SEI layers. The origin of stable Li cycling is closely related to the Li-ion diffusion mechanism via diverse crystalline grains and numerous grain boundaries in the fine crystalline-rich SEI layer. The results can elucidate a particular issue pertaining to the chemical structure of SEI layers that can induce uniform Li diffusion and rapid Li-ion conduction on Li metal anodes, developing stable Li metal batteries.**

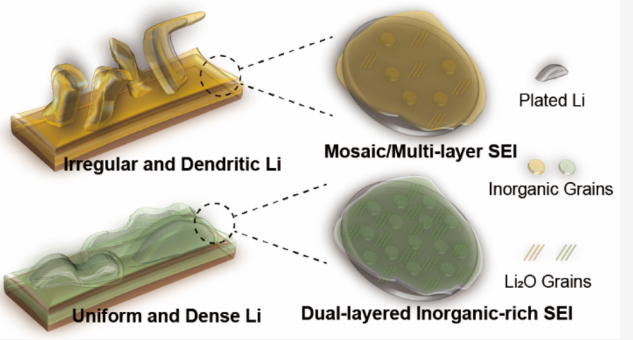

Metallic Li is well-known for the highest specific capacity (3,860 mAh g^{-1}) and the lowest redox potential (−3.040 V vs standard hydrogen electrode) among battery anode materials, making it ideal for developing high energy density battery systems, such as Li−O_2 (∼3,500 Wh kg^{-1}), Li−S (∼2,600 Wh kg^{-1}), and other future battery systems. Nevertheless, highly reactive Li undergoes continuous side reactions with electrolytes, which accelerate the loss of fresh Li source and electrolyte components, resulting in low Coulombic efficiencies and short cycle lives.[1−6] In particular, dendrites resulting from the spatial heterogeneity of the Li-ion distribution on the electrode surface can cause an internal short circuit in the battery system. It is believed that heterogeneous the solid electrolyte interphase (SEI) layer originating from the electrolyte component reduction contributes significantly to the issues mentioned above.[7−10]

Various strategies for improving the Li metal anode, such as using advanced electrolytes, enhance the electrochemical performance of Li metal batteries.[11] High-concentration electrolytes are known to reduce the average ion concentration gradients from the bulk electrolyte to the electrode surface. The smoothed concentration gradient from a bulk electrolyte to a current collector can facilitate stable metal deposition with a relatively large size, no discernible morphology, and no preferred growth direction.[6,12]

Fundamentally, the effect of the SEI layer formed on the electrode surface is as important as the relieved electrolyte concentration gradient for stable metal deposition.[13−15] Variables, such as surface and crystal free energy, govern the Li metal deposition on a foreign substrate surface.[16] Due to the presence of the electrolyte reductive reaction, the interfacial state would significantly impact these free energies during the Li deposition process. Since Li ions or electrolyte components react indiscriminately, it is challenging to comprehend the complicated interfacial reactions, including the correlation between Li deposition and SEI formation.

Although interfacial analyses, such as X-ray photoelectron spectroscopy (XPS), can infer the elemental composition change in the entire SEI layer, a proper analysis is required to

Received: March 9, 2023
Accepted: April 12, 2023
Published: April 13, 2023

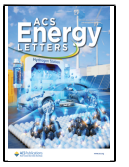

https://doi.org/10.1021/acsenergylett.3c00505
ACS Energy Lett. 2023, 8, 2193−2200

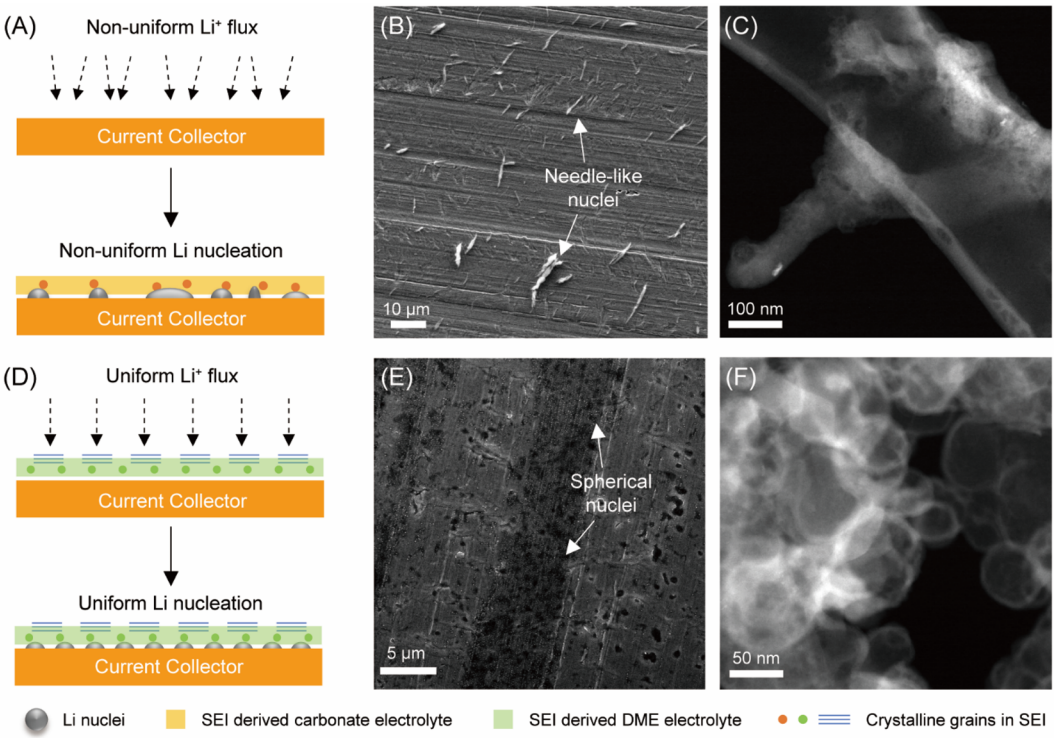

Figure 1. Li metal nucleation under different Li-flux conditions at the initial stage at 10 s. (A) Schematic of the nonuniform Li-ion flux near the current collector without the SEI layer contribution in the conventional carbonate electrolyte. (B and C) SEM (B) and Cryo-TEM (C) image of nonuniform Li nucleation on the copper current collector in the conventional carbonate electrolyte. (D) Schematic of the uniform Li-ion flux near the current collector with the abundant SEI layer in the high-concentration DME electrolyte. (E and F) SEM (E) and Cryo-TEM (F) image of uniform Li nucleation on the copper current collector in the high-concentration DME electrolyte.

comprehend the locally formed interface, the structural change of SEI layers, and plated Li.[17−19] Cryogenic transmission electron microscopy (Cryo-TEM) was introduced to the energy field originaally by the biology community.[17,18] The beam-sensitive Li has been investigated by this technique, which preserves structural/chemical information at low temperatures (<−170 °C) under relatively low-dose rates (<1,000 e·Å^{-2}·s^{-1}). Although cryogenic treatment stabilizes the analysis conditions, some difficulties persist. Each crystalline grain, such as Li_2O and LiF, may have different degrees of endurance to the high energy electron beam even under the same cryogenic conditions, which means much attention is needed to observe various crystalline inorganic grains that could have been formed during the cycling. Because of its complex amorphous and mixed crystalline structure, it is challenging to reveal the exact effect of the SEI layers on Li metal anodes.[20,21]

Herein, we have successfully studied the impacts of interfacial layers on the Li metal anode by comparing the structural/chemical properties using Cryo-TEM and density functional theory (DFT) calculations. Small and uniformly distributed Li nuclei were observed with the inorganic-rich SEI layers when a concentrated electrolyte was used. At the initial stage, the spatially homogeneous Li nuclei were deposited by uniform Li-ion migration via a rapidly formed high ionic conducting SEI layer, which could inhibit dendrite growth. In a subsequent charging process, the formed inorganic interphase grew into a compact dual-layered inorganic-rich SEI layer that can provide fast Li-ion pathways. Consequently, depending on the electrolyte system, this structural/chemical observation can provide profound insight and facilitate the design of superior Li metal batteries.

Uniform Li-Ion Flux and Nucleation in Inorganic-Rich SEI Layers. When a current is applied, Li ions near the surface of the current collector are consumed by transferred electrons with reductive reactions like SEI formation. Properties of SEIs, including the ionic conductivity, can change depending on their structure/chemical composition. It is well-known that the SEI layer derived from the conventional carbonate electrolyte has a mosaic or a multilayer structure with Li_2O crystalline grains embedded in an amorphous matrix. Although SEIs derived from carbonate electrolytes can be controlled by salt tuning, most of them have an amorphous-rich carbon matrix with heterogeneously precipitated inorganic components.[7,19,22] Li ions showed different conduction through the amorphous matrix and the inorganic crystalline grains of these SEIs, creating partially fast ionic conductive regions and uneven Li-ion diffusion over the entire SEI (Figure 1A).[23] The nonuniform Li-ion diffusion generated partially concentrated regions near the current collector. Finally, a nonuniform Li nucleation occurred at the initial stage of Li deposition as shown in Figures 1B,C and S1. Compared with the conventional carbonate electrolyte, LiFSI-DME based concentrated electrolyte demonstrated a different decomposition mechanism and rendered a robust inorganic-rich SEI layer.[11] Since DME solvent is chemically stable against reductive reaction, the formed SEI layer is composed of diverse inorganic species, such as Li_2O and LiF, that originated from the LiFSI decomposition (Figure 1D).[24] The SEI layer derived from concentrated electrolytes can deposit first or co-deposit with Li on the current collector since the LiFSI salt decomposes at a

https://doi.org/10.1021/acsenergylett.3c00505
ACS Energy Lett. 2023, 8, 2193−2200

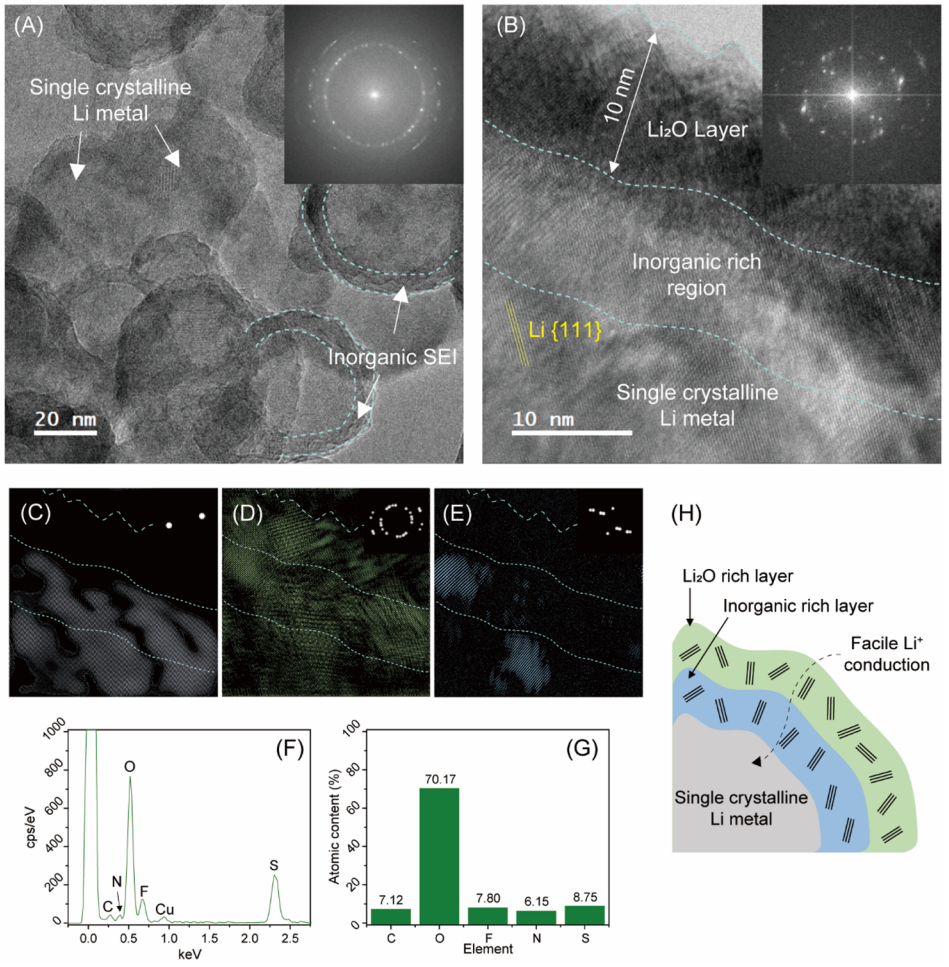

Figure 2. Inorganic-rich SEI layer in the high-concentration DME electrolyte. (A) Cryo-HRTEM image of spherical Li nuclei and inorganic-rich SEI layers (inset corresponds to the FFT) at the initial stage (2.0 mA·cm^{-1}, 10 s) in the high-concentration DME electrolyte. (B) Cryo-HRTEM image of the dual-layered inorganic-rich SEI layer after charging 1.0 mAh·cm^{-1} by 2.0 mA·cm^{-1} in the high-concentration DME electrolyte. (C−E) Areal distribution of deposited Li metal (C), Li_2O (D), LiF, Li_2S, and Li_3N (E) in the Cryo-HRTEM image shown in panel B. (F and G) TEM-EDS peaks of each element (F) and atomic content (G) in the dual-layered inorganic-rich SEI. (H) A schematic of the structure of the dual-layered inorganic-rich SEI.

relatively higher potential than Li nucleation. At the initial stage, the formed inorganic-rich SEI layer could regulate Li-ion diffusion evenly because of the abundantly distributed inorganic species over the entire SEI layer. The uniform Li-ion diffusion could facilitate smaller and more uniform nuclei in comparison to those formed using conventional carbonate electrolytes, as shown in Figures 1E,F and S1.

The crystal free energy, ΔG, is given by $\Delta G = 4\pi r^2\gamma + 4/3\pi r^3\Delta G_v$, where r is the radius of a spherical particle, γ the surface energy, and ΔG_v the free energy of the bulk crystal. The bulk crystal energy, ΔG_v, is expressed as $-k_B T\cdot\ln(S)\cdot v^{-1}$, which is defined by the Boltzmann's constant (k_B), temperature (T), the supersaturation of the solution (S), and molar volume (v). Overcoming the surface free energy is the most important factor for the uniform metal nucleation and growth on a foreign surface.[25] A high concentration of Li ions increases the supersaturation value on the Cu current collector in a concentrated DME electrolyte. Furthermore, the inorganic-rich SEI layer capable of inducing a fast Li-ion diffusion may affect the surface energy of the current collector with its lithiophilic property. Unlike the conventional electrolyte system, the concentration of Li ions near the current collector would not significantly be localized in the concentrated electrolyte systems. Evenly distributed Li ions did not trigger Li depletion across the entire regions under the same current density, resulting in an even distribution of small nuclei with the SEI abundant regions (Figures 1E,F and S1). These results suggest that the concentrated electrolytes can form the SEI more easily than conventional carbonate electrolytes at the initial stage and the formed interphase can regulate the initial nucleation uniformly (Figure 1C,F).

Nanoarchitecture of Inorganic-Rich SEI Derived from the LiFSI-DME Electrolytes. The initially formed SEI layer played an important role in the subsequent cycles of Li plating and stripping. The nuclei formed in the conventional carbonate electrolyte showed diverse morphological properties such as mossy-like nuclei of 50−200 nm, which were aggregated in most parts of the Li deposition (Figures 1B and S1). Some large needle-like nuclei over 400 nm without a specific SEI layer were observed at a specific area on the current collector (Figure 1C). This needle-like structure confirmed that Li is governed by the kinetically preferential deposition on the existing nucleation sites. The amorphous-rich mosaic and multilayer SEIs, mostly composed of carbon species derived from carbonate solvent, showed uneven nanostructure through the entire electrode surface (Figures S2−S4). The regions of

https://doi.org/10.1021/acsenergylett.3c00505
ACS Energy Lett. 2023, 8, 2193−2200

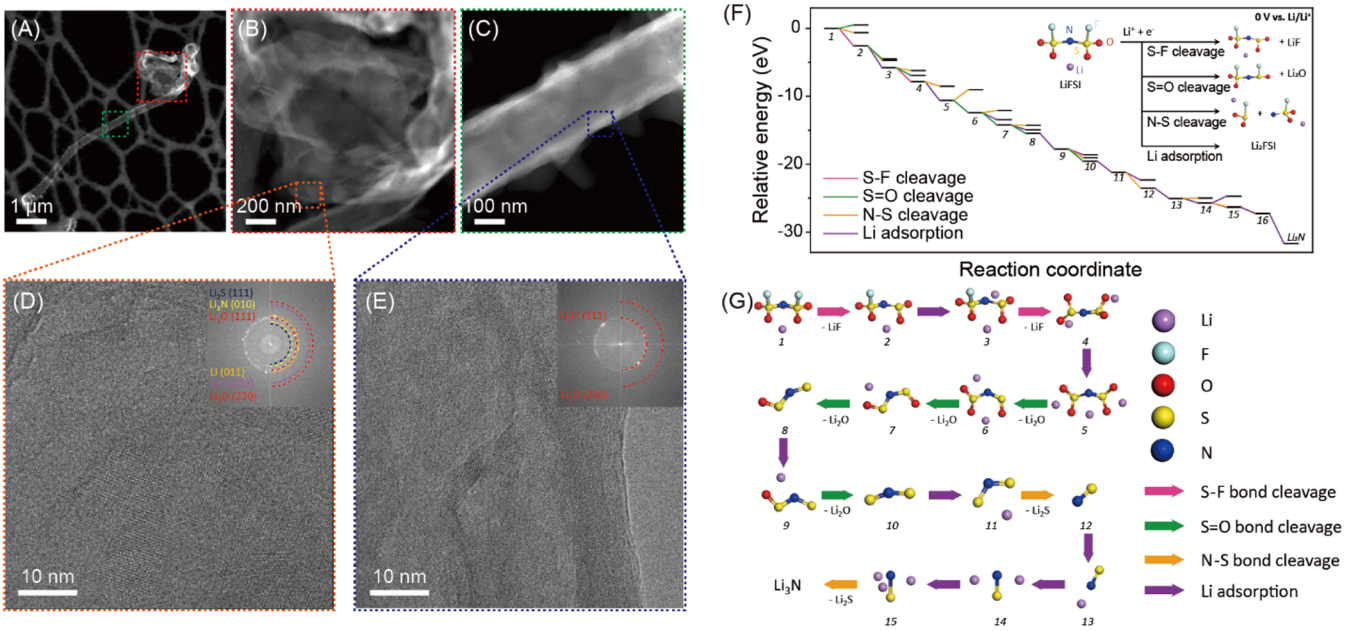

Figure 3. Mixed morphology of deposited Li in 2.0 M LiFSI DME electrolyte and decomposition mechanism of LiFSI salt. (A) Low-magnification Cryo-TEM image of the deposited Li metal with mixed morphology of dendrite and nanosheet in 2.0 M LiFSI DME electrolyte. (B) Deposited Li metal with the nanosheet morphology (red dashed box in panel A). (C) Deposited Li metal with the dendrite morphology (green dashed box in panel A). (D) Cryo-HRTEM image of the nanosheet Li metal and SEI layer (orange dashed box in panel B). The inset corresponds to the FFT. (E) Cryo-HRTEM image of the dendrite Li metal and SEI layer (blue dashed box in panel C). The inset corresponds to the FFT. (F) LiFSI salt decomposition potential energy diagram and (G) schematic decomposition mechanisms that formed the dual-layered inorganic-rich SEI layer in the concentrated DME electrolyte.

unevenly embedded crystalline inorganic species or partially covered Li_2O could provide unstable spots for dendritic growth in the subsequent cycles. The heterogeneously formed Li nuclei and SEI layer in conventional carbonate electrolytes could cause the focused Li flux and yield higher local current densities over the limiting value to initiate the tip-growing Li dendrite (Figure S5a,b).[12,26] However, the uniform Li diffusion through an inorganic-rich SEI layer derived from the concentrated electrolyte generated a peculiar shape of Li nuclei (Figures 1F and 2A). Approximately 5 nm-thick distinct layers composed of Li_2O, LiF, and sulfide species were observed on the surface of the spherical nuclei, as shown in Figure 2A. The strong diffraction spots of sulfide species, Li_2O, and LiF as shown in Figure S6a suggest that the inorganic species were mainly formed and facilitated the uniform Li diffusion at the initial stage of Li deposition. These inorganic species in the SEI layer which have high ionic conductivity compared with the amorphous matrix divided the focused Li flux and evenly made small nuclei of approximately 50 nm. The uniformly formed spherical nuclei and SEI layer can further guide Li ions evenly through the entire surface in subsequent cycles and make stable electroplating possible. According to the LaMer mechanism, the concentration of ions at the surface decreases rapidly when the initial nucleation occurs. If a sufficiently high concentration of ions can be maintained, the nucleation is uniform and stable upon further plating because ion diffusion for crystal growth is supplied smoothly.[6] Small single-crystalline spherical nuclei grew to nanosheet-like Li, not dendrites (Figure S5c,d), with the abundant inorganic-rich SEI layer composed of the Li_2O outer layer and the inorganic-rich inner layer (Figures 2B and S6b). The Li_2O layer existed evenly, approximately 10 nm above the deposited Li metal, and other inorganic components such as LiF, Li_2S, and Li_3N were approximately 5 nm inside the Li metal. This unique dual-layered nanostructure derived from the concentrated electrolyte showed a lot of inorganic crystalline grains, different from the conventional carbonate electrolyte SEI layer (Figures 2B and S2). The distribution of each component was also revealed by areal distribution mapping data as shown in Figure 2C (Li metal), 2D (Li_2O), and 2E (LiF, Li_2S, and Li_3N) consistent with the results of TEM-EDS and XPS-depth profile data (Figures 2F,G, S7, and S8). Li ions can find diverse fast pathways through the grain boundaries among many inorganic crystalline grains with migration energy barriers lower than bulk grains or amorphous matrix (Figure 2H).[27] The fact that some inorganic components except Li_2O were placed partially concentrated at the specific areas might be a starting point for the morphological evolution from spherical nuclei to nanosheet. The unique SEI layer was also different with relatively low-concentration electrolytes such as 2.0 M LiFSI-DME as shown in Figure 3A. The deposited Li using a 2.0 M electrolyte showed a mixed morphology of nanosheet (Figure 3B, red square in Figure 3A) and dendrite (Figure 3C, green square in Figure 3A). The surface of the nanosheet consisted of diverse inorganic products, such as Li_2S, Li_3N, and Li_2O, like the interface of the deposited Li using highly concentrated electrolyte (Figures S6b and 3D). However, the interfacial structure of the dendrite contained only Li_2O comparable to the dendrite-dominated Li deposition in conventional carbonate electrolytes (Figures S2 and 3E). These results confirm that the inorganic-rich SEI layer can induce more uniform and denser Li deposition.

DFT study was further conducted to reveal the formation mechanism of the dual-layered inorganic-rich SEI.[28,29] The main components of the inorganic-rich SEI layer were LiF, Li_2S, and Li_3N, the decomposition products of LiFSI salt. After

https://doi.org/10.1021/acsenergylett.3c00505
ACS Energy Lett. 2023, 8, 2193−2200

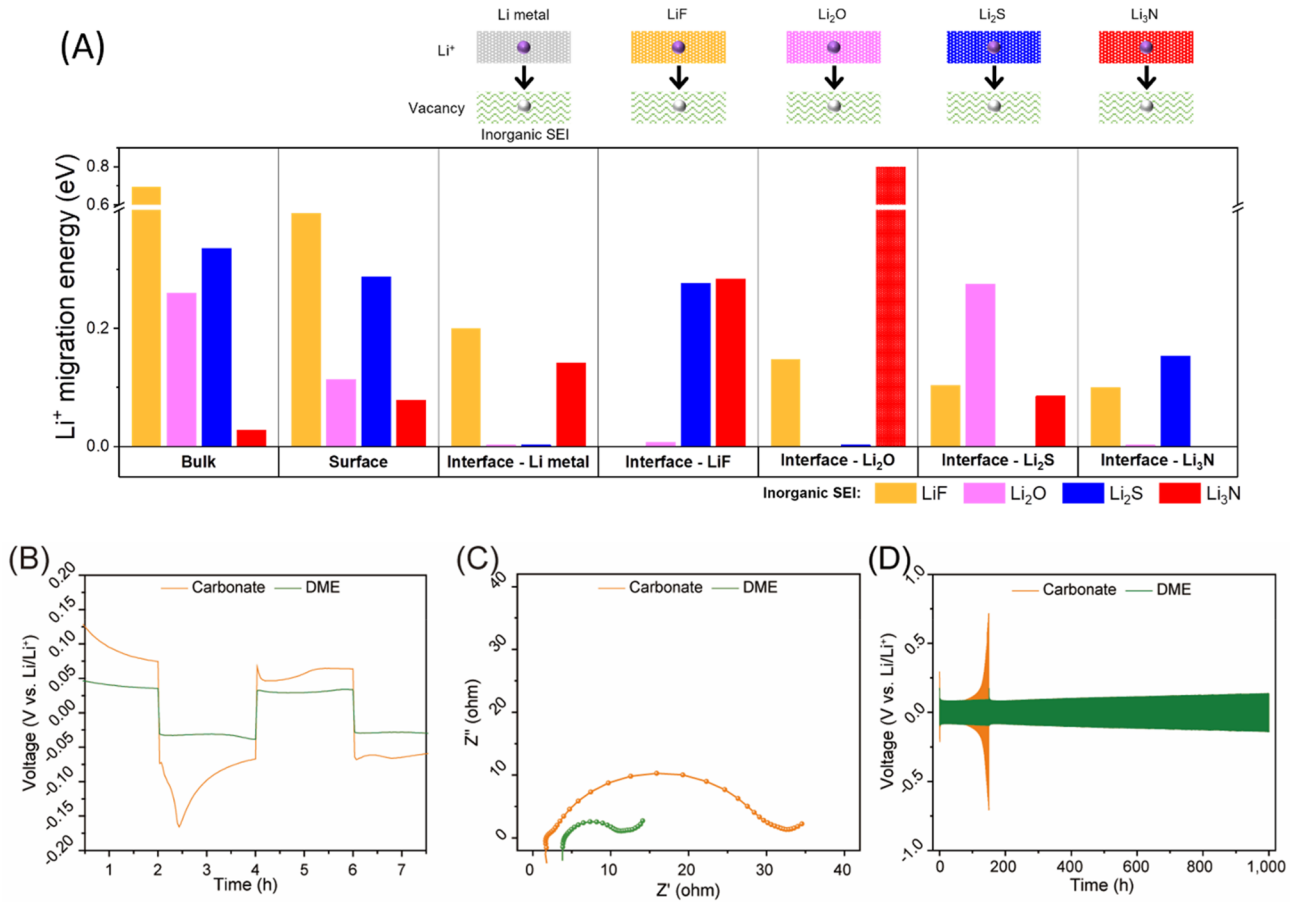

Figure 4. Fast Li-ion conduction through the inorganic-rich SEI layer. (A) Li-ion migration energy comparison through the bulk, surface structure of inorganic grains, and interface among crystalline grains. Li-ion migration energy between the same phase was not considered (displayed as a gap in each column). Large migration energy of Li_3N−Li_2O is the reverse direction energy barrier of spontaneous reaction (see the Molecular Modeling section in the Supporting Information and Figures S12−S14). (B) Comparison of overpotential in the initial stage using different electrolytes. (C) EIS data after the first charging on the copper current collector. (D) Li symmetric cell data under 1.0 mAh·cm^{-1} by 2.0 mA·cm^{-1}.

reducing the LiFSI with additional Li ions, the S—F, S═O, and N—S chemical bonds broke, making their products the seeds of inorganic compounds in the SEI. We evaluated the thermodynamic stability of those products after reducing LiFSI salt with extra Li ions. As a result, S—F bonds broke first before any other bonds, and S═O and N—S bonds broke consecutively (Figure 3F,G). The N—S bond broke at the latter phase to produce Li_2S and Li_3N, which is predicted to be the potential-determining step of LiFSI decomposition (Figure S9). During the LiFSI decomposition process, Li ions exhibited a preference for bondingwith the inorganic species rather than breaking extra chemical bonds when the molecular neutrality of the salt was lost. Thus, LiF, Li_2O, Li_2S, and Li_3N were produced rapidly with the Li nucleation and distributed near the deposited Li metal. In the additional Li growth process where sufficient overpotential is maintained, LiF and Li_2O are expected to compose the outer layer because of the continuously applied potential, breaking the N—S bond harder. This predicted decomposition process is consistent with the nanoarchitecture of the dual-layered inorganic-rich SEI as shown in Figure 2B.

Electrochemical Performance and Long-Term Durability of Li Metal Batteries. To elucidate the high ionic conductivity of the inorganic-rich SEI layer, DFT calculations were performed.[30,31] The bulk inorganic SEI species and their surface/interfaces were considered possible ionic conducting hosts. Among the bulk inorganic SEI layers, LiF showed the lowest Li-ion conductivity, while Li_3N has a high Li-ion conducting channel along specific interlayer diffusion (Figure 4A). The Li_2O and Li_2S bulk structure showed 0.26 and 0.34 eV of energy barrier, indicating it is relatively difficult to transfer Li ions. In most cases, Li-ion diffusion along the surface planes is faster than that through the bulk region. Although a relatively low energy barrier was observed in the Li_3N bulk, Li_3N surface, and Li_2O surface structures, they are not the main reason for the improved electrochemical performance. When Li ions were transferred from the Li_2O-rich outer layer into the Li metal side, Li ions would encounter various pathways which have diverse energy barriers (see interface section in Figure 4A). Numerous grain boundaries formed among many crystalline grains could considerably affect Li conduction through their lower energy barrier. Interestingly, most interfacial diffusion among inorganic species showed a low energy barrier (less than 0.2 eV), which is similar to the Li_2O surface structure. If Li ions exist at the bulk structure or near the surface plane of SEI species with a high energy barrier, Li ions can be easily transferred to the interfacial sites among crystalline grains that have a lower migration energy barrier. In other words, efficient and fast Li

https://doi.org/10.1021/acsenergylett.3c00505
ACS Energy Lett. 2023, 8, 2193−2200

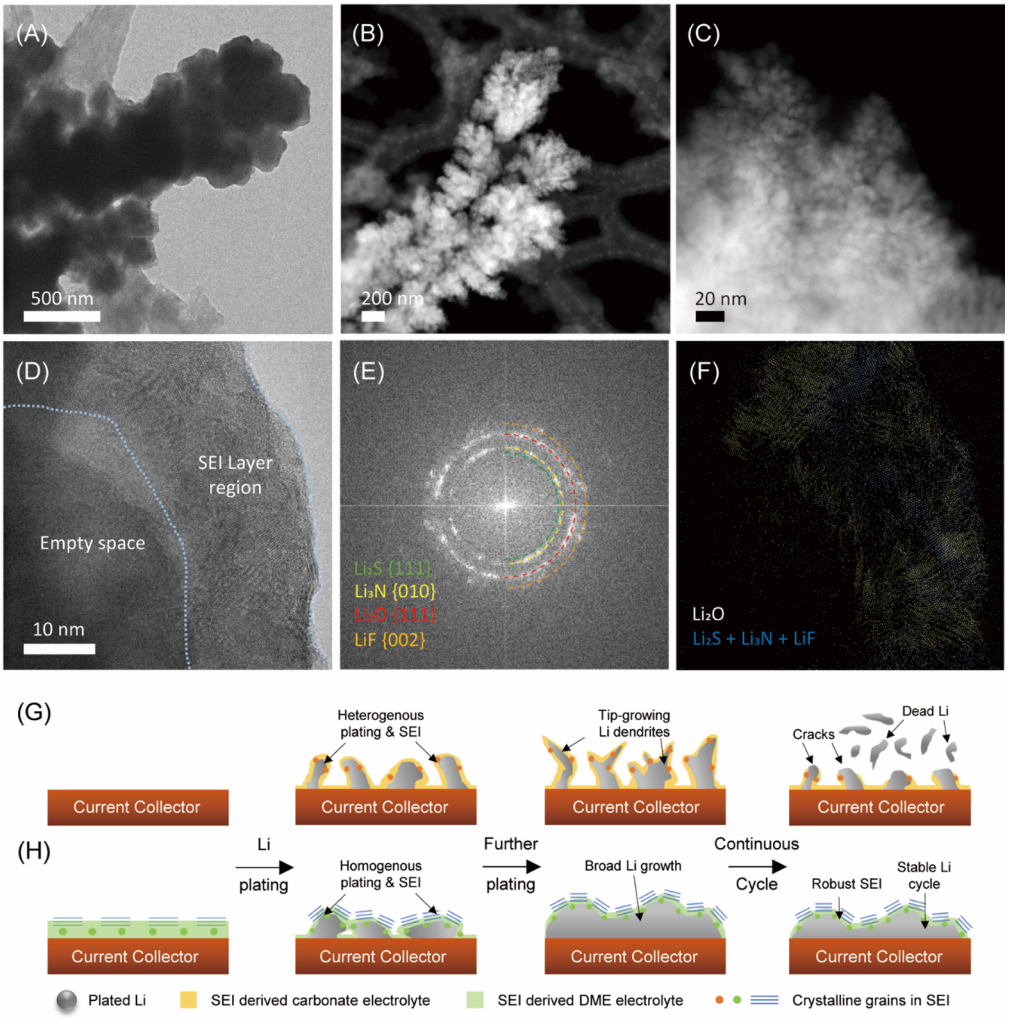

Figure 5. Uniform Li stripping through an inorganic-rich SEI layer. (A–C) Low magnification Cryo-TEM and high magnification Cryo-STEM images of the remaining SEI layer after the discharge process in the high-concentration DME electrolyte system. (D) Cryo-HRTEM image of the remaining SEI layer and empty space inside the layer in the high concentration DME electrolyte system. (E) FFT image containing an inorganic component in panel D. (F) Areal distribution of the inorganic-rich SEI layer in panel D. (G and H) Schematic of Li growth/stripping mechanisms during continuous cycles (G) with nonuniform and (H) uniform SEI layers.

conduction could be achieved in the inorganic-rich dual-layered SEI.

This different SEI layer significantly affected the electrochemical performance of symmetric Li cells, as shown in Figure 4B–D. The overpotential of the concentrated electrolyte system was approximately 30 mV, which is 5–6 times lower than that of the conventional carbonate electrolyte system in the first Li nucleation, and remained unchanged in subsequent cycles (Figure 4B). However, a large voltage spike of the conventional carbonate electrolyte system at the initial stage suggests that the interphase composed of inorganic species effectively decreased the electrode polarization from the initial stage. We further confirmed the contribution of the dual-layered inorganic-rich SEI to the electrochemical impedance spectroscopy (EIS) after the first deposition on a bare Cu current collector using each electrolyte (Figure 4C). The semicircle from the conventional carbonate electrolyte system yielded a resistance of approximately 30.23 Ω, but the concentrated electrolyte system yielded 11.10 Ω with the help of the swiftly formed SEI layer. The robust SEI layer formed at the first cycle could lead to stable cycling over 1,000 cycles while maintaining low overpotential (Figure 4D). Although the ionic conductivity of the bulk electrolyte is relatively low due to high viscosity, the high ionic conductive SEI layer could decrease the overpotential and the resistance at the interface, as shown in Figure 4B,C. The role of fluoroethylene carbonate (FEC) additive in conventional carbonate electrolytes is to change the structure of the SEI layer upon Li metal increasing the Coulombic efficiency, but the cycle retention was not significantly improved at a relatively high current density of 2.0 mA·cm^{-2} (Figure S10a). Even with an FEC additive, a sharp dendritic shape inevitably formed during Li deposition which could provide a notch region at specific points in the subsequent cycles, resulting in cracks and dead lithium (Figure S5a,b).[8,9,19] The stability of Li metal anode using relatively low-concentration LiFSI-DME electrolyte was also poor as shown in Figure S10b. Low overpotential during the cycles indicated that the electrolytes can facilitate rapid transfer of Li ions due to the thin SEI layer composed of high ionic conductive species (Figure S10c,d). However, Li symmetric cells with 1.0 and 2.0 M LiFSI-DME electrolyte showed a short-circuit failure near 200 cycles (Figure S10e) because they showed an identical nanostructure

https://doi.org/10.1021/acsenergylett.3c00505
ACS Energy Lett. 2023, 8, 2193–2200

of the SEI layer and dendritic Li deposition after the charge process (Figures 3C and S11).

Furthermore, a different Li cycling occurred in the concentrated electrolyte system because the robust dual inorganic layer was well-maintained even after the stripping process (Figure 5A–C). The deposited nanosheet showed shrinkage, forming clusters of approximately 200 nm during the discharge process, as shown in Figure 5A. In high-magnification STEM images (Figure 5B,C), the clusters are composed of many small spheres, similar to the deposited Li at the initial stage. After the discharge process at a potential exceeding 1.0 V, an empty space was created where Li was originally present, and a distinct SEI shell with a similar nanostructure to the SEI layer formed on the deposited Li metal during the charge process (Figure 5D). According to the FFT patterns, inorganic components such as Li_2S, Li_3N, Li_2O, and LiF were maintained abundantly even after the complete stripping process of Li (Figure 5E). The robust structural configuration of the SEI layer that consists of high ionic conductive inorganic components covered with an Li_2O layer was intact as shown in the areal distribution mapping data (Figure 5F). Although some structural changes occurred during the stripping process from the dual-layered structure to the wrapped structure, the remaining specific shell confirmed the rigid and compact nature of the inorganic-rich SEI layer. Homogeneously spread clusters covered by an SEI shell may act as nucleation sites in the subsequent process because of the well-maintained Li conductive layer with the empty space for Li deposition. In the conventional carbonate electrolyte system, heterogeneous Li cycling such as tip-growing and crack formation would be repeated since the formed nonuniform SEI layer could not balance the Li flux (Figure 5G). Otherwise, a regulated Li flux through the rapidly formed robust inorganic-rich SEI layer facilitated an evenly distributed and stable Li cycling. This functional difference in the SEI layer affected not only the initial Li nucleation but also the stable and dense Li packing during the continuous cycles (Figure 5H). The distinct structural advantages of a dual-layered inorganic-rich SEI clarify the electrolyte engineering to establish stable Li metal batteries.

In this work, we reveal the exact nanostructure of the SEI layer on the Li metal anode and its fundamental effect on stable Li metal batteries by Cryo-TEM and DFT analysis. Using a proper dose rate of Cryo-TEM can provide the fine atomic structure of a dual-layered inorganic-rich SEI and explain the difference with the SEI layer in the conventional carbonate electrolyte system. Unlike previous studies, we also reveal that a concentrated electrolyte used in this work can generate not the fluorine-rich SEI but the unique structure of the SEI layer. Furthermore, a fundamental understanding of the formation of high ionic conductive inorganic species from the LiFSI decomposition process could give insights into future development of superior SEI layers for Li metal batteries.

■ ASSOCIATED CONTENT

Supporting Information

The Supporting Information is available free of charge at https://pubs.acs.org/doi/10.1021/acsenergylett.3c00505.

Experimental section, details of DFT calculations, additional SEM images, additional Cryo-HRTEM images, TEM-EDS data, XPS results, additional FFT pattern of Cryo-HRTEM images, DFT calculations of LiFSI salt decomposition, additional Li-symmetric cell performance (PDF)

■ AUTHOR INFORMATION

Corresponding Authors

Sang Kyu Kwak − *Department of Chemical and Biological Engineering, Korea University, Seoul 02841, Republic of Korea;* orcid.org/0000-0002-0332-1534; Email: skkwak@korea.ac.kr

Hyun-Wook Lee − *School of Energy and Chemical Engineering, Ulsan National Institute of Science and Technology (UNIST), Ulsan 44919, Republic of Korea;* orcid.org/0000-0001-9074-1619; Email: hyunwooklee@unist.ac.kr

Authors

Tae-Ung Wi − *School of Energy and Chemical Engineering, Ulsan National Institute of Science and Technology (UNIST), Ulsan 44919, Republic of Korea; Department of Chemical and Biomolecular Engineering, Rice University, Houston, Texas 77005, United States*

Sung O Park − *Department of Materials Science and Engineering, Seoul National University, Seoul 08826, Republic of Korea*

Su Jeong Yeom − *School of Energy and Chemical Engineering, Ulsan National Institute of Science and Technology (UNIST), Ulsan 44919, Republic of Korea;* orcid.org/0000-0002-3545-3232

Min-Ho Kim − *School of Energy and Chemical Engineering, Ulsan National Institute of Science and Technology (UNIST), Ulsan 44919, Republic of Korea*

Imanuel Kristanto − *Department of Chemical and Biological Engineering, Korea University, Seoul 02841, Republic of Korea*

Haotian Wang − *Department of Chemical and Biomolecular Engineering, Rice University, Houston, Texas 77005, United States;* orcid.org/0000-0002-3552-8978

Complete contact information is available at: https://pubs.acs.org/10.1021/acsenergylett.3c00505

Notes

The authors declare no competing financial interest.

■ ACKNOWLEDGMENTS

This work is supported by the 2023 Research Fund (1.230040.01) of UNIST, Individual Basic Science & Engineering Research Program (RS-2023-00208929 and 2021R1C1C2004527) through the National Research Foundation (NRF) of Korea funded by the Ministry of Science and ICT (MSIT), the Ministry of Trade, Industry & Energy/Korea Institute of Energy Technology Evaluation and Planning (MOTIE/KETEP) (20214000000660). Computational resources were provided by the Korea Institute of Science and Technology Information (KISTI) (KSC-2022-CRE-0110). This study contains results obtained by using the equipment of UNIST Central Research Facilities (UCRF).

■ REFERENCES

(1) Dunn, B.; Kamath, H.; Tarascon, J. M. Electrical energy storage for the grid: A battery of choices. *Science* **2011**, *334*, 928–935.

(2) Lin, D.; Liu, Y.; Cui, Y. Reviving the Lithium Metal Anode for High-Energy Batteries. *Nat. Nanotechnol.* **2017**, *12* (3), 194–206.

(3) Yan, K.; Lu, Z.; Lee, H.-W.; Xiong, F.; Hsu, P.-C.; Li, Y.; Zhao, J.; Chu, S.; Cui, Y. Selective Deposition and Stable Encapsulation of Lithium through Heterogeneous Seeded Growth. *Nat. Energy* **2016**, *1* (3), 16010.
(4) Tang, W.; Yin, X.; Kang, S.; Chen, Z.; Tian, B.; Teo, S. L.; Wang, X.; Chi, X.; Loh, K. P.; Lee, H. W.; Zheng, G. W. Lithium Silicide Surface Enrichment: A Solution to Lithium Metal Battery. *Adv. Mater.* **2018**, *30* (34), 1801745.
(5) Go, W.; Kim, M. H.; Park, J.; Lim, C. H.; Joo, S. H.; Kim, Y.; Lee, H. W. Nanocrevasse-Rich Carbon Fibers for Stable Lithium and Sodium Metal Anodes. *Nano Lett.* **2019**, *19* (3), 1504−1511.
(6) Xiao, J. How Lithium Dendrites Form in Liquid Batteries. *Science* **2019**, *366* (6464), 426−427.
(7) Peled, E. The Electrochemical Behavior of Alkali and Alkaline Earth Metals in Nonaqueous Battery Systems—The Solid Electrolyte Interphase Model. *J. Electrochem. Soc.* **1979**, *126* (12), 2047−2051.
(8) Sacci, R. L.; Black, J. M.; Balke, N.; Dudney, N. J.; More, K. L.; Unocic, R. R. Nanoscale Imaging of Fundamental Li Battery Chemistry: Solid-Electrolyte Interphase Formation and Preferential Growth of Lithium Metal Nanoclusters. *Nano Lett.* **2015**, *15* (3), 2011−2018.
(9) Li, T.; Zhang, X. Q.; Shi, P.; Zhang, Q. Fluorinated Solid-Electrolyte Interphase in High-Voltage Lithium Metal Batteries. *Joule* **2019**, *3* (11), 2647−2661.
(10) Kim, S.; Park, S. O.; Lee, M. Y.; Lee, J. A.; Kristanto, I.; Lee, T. K.; Hwang, D.; Kim, J.; Wi, T. U.; Lee, H. W.; Kwak, S. K.; Choi, N. S. Stable Electrode−Electrolyte Interfaces Constructed by Fluorine- and Nitrogen-Donating Ionic Additives for High-Performance Lithium Metal Batteries. *Energy Storage Mater.* **2022**, *45*, 1−13.
(11) Qian, J.; Henderson, W. A.; Xu, W.; Bhattacharya, P.; Engelhard, M.; Borodin, O.; Zhang, J.-G. High Rate and Stable Cycling of Lithium Metal Anode. *Nat. Commun.* **2015**, *6* (1), 6362.
(12) Chen, S.; Zheng, J.; Yu, L.; Ren, X.; Engelhard, M. H.; Niu, C.; Lee, H.; Xu, W.; Xiao, J.; Liu, J.; Zhang, J. G. High-Efficiency Lithium Metal Batteries with Fire-Retardant Electrolytes. *Joule* **2018**, *2* (8), 1548−1558.
(13) Hobold, G. M.; Lopez, J.; Guo, R.; Minafra, N.; Banerjee, A.; Shirley Meng, Y.; Shao-Horn, Y.; Gallant, B. M. Moving beyond 99.9% Coulombic Efficiency for Lithium Anodes in Liquid Electrolytes. *Nat. Energy* **2021**, *6* (10), 951−960.
(14) Chen, H.; Pei, A.; Lin, D.; Xie, J.; Yang, A.; Xu, J.; Lin, K.; Wang, J.; Wang, H.; Shi, F.; Boyle, D.; Cui, Y. Uniform High Ionic Conducting Lithium Sulfide Protection Layer for Stable Lithium Metal Anode. *Adv. Energy Mater.* **2019**, *9* (22), 1900858.
(15) Zhang, X. Q.; Chen, X.; Xu, R.; Cheng, X. B.; Peng, H. J.; Zhang, R.; Huang, J. Q.; Zhang, Q. Columnar Lithium Metal Anodes. *Angew. Chemie - Int. Ed.* **2017**, *56* (45), 14207−14211.
(16) Thanh, N. T. K.; Maclean, N.; Mahiddine, S. Mechanisms of Nucleation and Growth of Nanoparticles in Solution. *Chem. Rev.* **2014**, *114* (15), 7610−7630.
(17) Fang, C.; Li, J.; Zhang, M.; Zhang, Y.; Yang, F.; Lee, J. Z.; Lee, M. H.; Alvarado, J.; Schroeder, M. A.; Yang, Y.; et al. Quantifying inactive lithium in lithium metal batteries. *Nature* **2019**, *572*, 511−515.
(18) Li, Y.; Li, Y.; Pei, A.; Yan, K.; Sun, Y.; Wu, C. L.; Joubert, L. M.; Chin, R.; Koh, A. L.; Yu, Y.; Perrino, J.; Butz, B.; Chu, S.; Cui, Y. Atomic Structure of Sensitive Battery Materials and Interfaces Revealed by Cryo−Electron Microscopy. *Science* **2017**, *358* (6362), 506−510.
(19) Li, Y.; Huang, W.; Li, Y.; Pei, A.; Boyle, D. T.; Cui, Y. Correlating Structure and Function of Battery Interphases at Atomic Resolution Using Cryoelectron Microscopy. *Joule* **2018**, *2* (10), 2167−2177.
(20) Han, B.; Li, X.; Bai, S.; Zou, Y.; Lu, B.; Zhang, M.; Ma, X.; Chang, Z.; Meng, Y. S.; Gu, M. Conformal Three-Dimensional Interphase of Li Metal Anode Revealed by Low-Dose Cryoelectron Microscopy. *Matter* **2021**, *4* (11), 3741−3752.
(21) Shadike, Z.; Lee, H.; Borodin, O.; Cao, X.; Fan, X.; Wang, X.; Lin, R.; Bak, S. M.; Ghose, S.; Xu, K.; Wang, C.; Liu, J.; Xiao, J.; Yang, X. Q.; Hu, E. Identification of LiH and Nanocrystalline LiF in the Solid−Electrolyte Interphase of Lithium Metal Anodes. *Nat. Nanotechnol.* **2021**, *16* (5), 549−554.
(22) Jurng, S.; Brown, Z. L.; Kim, J.; Lucht, B. L. Effect of Electrolyte on the Nanostructure of the Solid Electrolyte Interphase (SEI) and Performance of Lithium Metal Anodes. *Energy Environ. Sci.* **2018**, *11* (9), 2600−2608.
(23) Balazs, A. C.; Emrick, T.; Russell, T. P. Nanoparticle polymer composites: Where two small worlds meet. *Science* **2006**, *314*, 1107−11104.
(24) Zhang, X. Q.; Chen, X.; Hou, L. P.; Li, B. Q.; Cheng, X. B.; Huang, J. Q.; Zhang, Q. Regulating Anions in the Solvation Sheath of Lithium Ions for Stable Lithium Metal Batteries. *ACS Energy Lett.* **2019**, *4* (2), 411−416.
(25) Pei, A.; Zheng, G.; Shi, F.; Li, Y.; Cui, Y. Nanoscale Nucleation and Growth of Electrodeposited Lithium Metal. *Nano Lett.* **2017**, *17* (2), 1132−1139.
(26) Kushima, A.; So, K. P.; Su, C.; Bai, P.; Kuriyama, N.; Maebashi, T.; Fujiwara, Y.; Bazant, M. Z.; Li, J. Liquid Cell Transmission Electron Microscopy Observation of Lithium Metal Growth and Dissolution: Root Growth, Dead Lithium and Lithium Flotsams. *Nano Energy* **2017**, *32*, 271−279.
(27) Ramasubramanian, A.; Yurkiv, V.; Foroozan, T.; Ragone, M.; Shahbazian-Yassar, R.; Mashayek, F. Lithium Diffusion Mechanism through Solid-Electrolyte Interphase in Rechargeable Lithium Batteries. *J. Phys. Chem. C* **2019**, *123* (16), 10237−10245.
(28) Delley, B. An All-Electron Numerical Method for Solving the Local Density Functional for Polyatomic Molecules. *J. Chem. Phys.* **1990**, *92* (1), 508−517.
(29) Perdew, J. P.; Burke, K.; Ernzerhof, M. Generalized Gradient Approximation Made Simple. *Phys. Rev. Lett.* **1996**, *77* (18), 3865−3868.
(30) Klamt, A.; Schüürmann, G. COSMO: A New Approach to Dielectric Screening in Solvents with Explicit Expressions for the Screening Energy and Its Gradient. *J. Chem. Soc. Perkin Trans. 2* **1993**, No. 5, 799−805.
(31) Hall, D. S.; Self, J.; Dahn, J. R. Dielectric Constants for Quantum Chemistry and Li-Ion Batteries: Solvent Blends of Ethylene Carbonate and Ethyl Methyl Carbonate. *J. Phys. Chem. C* **2015**, *119* (39), 22322−22330.

https://doi.org/10.1021/acsenergylett.3c00505
ACS Energy Lett. 2023, 8, 2193−2200